

3D Based Landmark Tracker Using Superpixels Based Segmentation for Neuroscience and Biomechanics Studies

Omid Haji Maghsoudi
 Spence Lab., Bioengineering,
 Temple University,
 Philadelphia, PA, USA, 19122
 o.maghsoudi@temple.edu

Andrew Spence¹
 Spence Lab., Bioengineering,
 Temple University,
 Philadelphia, PA, USA, 19122
 http://www.spencelab.com

Abstract

Examining locomotion has improved our basic understanding of motor control and aided in treating motor impairment. Mice and rats are premier models of human disease and increasingly the model systems of choice for basic neuroscience. High frame rates (250 Hz) are needed to quantify the kinematics of these running rodents. Manual tracking, especially for multiple markers, becomes time-consuming and impossible for large sample sizes. Therefore, the need for automatic segmentation of these markers has grown in recent years. Here, we address this need by presenting a method to segment the markers using the SLIC superpixel method. The 2D coordinates on the image plane are projected to a 3D domain using direct linear transform (DLT) and a 3D Kalman filter has been used to predict the position of markers based on the speed and position of markers from the previous frames. Finally, a probabilistic function is used to find the best match among superpixels. The method is evaluated for different difficulties for tracking of the markers and it achieves 95% correct labeling of markers.

1. Introduction

Studying animal, including humans, locomotion has been one of the challenging areas in the modern science. Our health and well-being are directly linked with movement. Animal movement can explain some biological world phenomena. In addition, it can impact the treatment of musculoskeletal injuries and neurological disorders, improve prosthetic limb design, and aid in the construction of legged robots [24].

The intentional changes in an animal gait, the timing of paw motion relative to each other using by the animal [6], can be seen during movement. The animal movement can

be perturbed using an internal or external perturbation. A mechanical perturbation (e.g., earthquake) while the animal is running, for example, deflecting the surface during running, or an electrical stimulation applied to the nervous system, or even the application of new genetically targeted techniques, like optogenetics [5] or designer receptors exclusively activated by designer drugs [36], are several of the increasingly sophisticated methods applying perturbations that dissect the movement control.

To study the gait and kinematics, it is needed to track specific landmarks on the body of an animal. Tracking of these landmarks on the body of animal relies on shaving fur, drawing markers on the skin, attaching retroreflective markers, or manual clicking by a user for consecutive frames[25]. The attachment of retroreflective markers can be impossible in many cases as animals, like rats and mice, start grooming and chewing the markers. Therefore, shaving fur and drawing markers can be the most reliable method for tracking of specific landmarks [37].

Commercially available systems (Digigait [7, 9, 30], Motorater [33], Noldus Catwalk [6, 13, 17, 31]) are prohibitively expensive, and may only provide information about paws during the stance phase which makes them limited for some studies. In addition, some computerized methods (simple thresholding, cross-correlation, or template matching) have been proposed to answer this need. However, manual clicking can be considered the usual method to track the markers [15]. Therefore, the need for a robust method to help neuroscientists and biologists have been felt.

Tracking has been a recently popular topic in image processing. Many methods have been developed for different applications; cell migration tracking [32], human tracking [22], and diseases frames tracking in consecutive frames [10, 27]. Tracking methods should be developed based on conditions governing around a specific problem which make them unique [11].

As discussed, locomotion analysis needs to track some landmarks on the body of an animal. The 2D tracking from the frames can provide the required knowledge to examine

¹This material is based upon work supported by, or in part by, the U.S. Army Research Laboratory and the U. S. Army Research Office under contract/grant number W911NF1410141, proposal 64929EG, to A. Spence.

the animal’s gait. However, access to 3D information can improve our understanding about locomotion including roll, pitch, and yaw [28].

We presented a superpixel based segmentation method to find the markers following by a weighted 2D tracker [26]. The results were so promising and it inspired us to use the SLIC method for segmentation. The tracker was using 2D information from an image plane to find the position of landmarks for consecutive frames. However, the latest issue caused problems for tracking of landmarks when they were occluding by the body or another limb, getting too close to another landmark, or having some dirt on the plexy glass.

Here we take the advantage of superpixels for segmentation of landmarks, with a small difference compared to [26]. However, the main contribution of this study is a robust tracker design to resolve the limitations of our previously presented method. We find the solution in using of 3D information and processing two camera information at the same time. 3D Kalman filter and direct linear transform were used to achieve this goal.

2. Methods

2.1. Camera and Treadmill Setup

Four side view cameras were used to capture video from a treadmill located in the middle of capturing area. The cameras were synchronized using an external pulse generator inducing a 250 HZ pulse to assure they were captured at the same time. In addition, the frames were labeled by a UTC time provided the pulse generator to not miss a single frame. The capture time for each trial was 4 seconds providing 1000 frames. The frames were Bayer encoded and we use a debayering function to convert them to RGB color space frames [25].

We converted the frames from the RGB color space to the HSV color space because it places all color information in a single channel, as compared to the RGB or the LAB colors spaces [12, 23].

2.2. Superpixel Segmentation

Superpixels contract and group uniform pixels in an image and have been widely used in many computer vision applications such as image segmentation [20, 29]. the outcome is more natural and perceptually meaningful representation of the input image compared to pixels. Different approaches have been developed to generate superpixels: normalized cuts [35], mean shift algorithm [4], graph-based method [8], Turbopixels [19], SLIC superpixels [1], and optimization-based superpixels [41]. Simple linear iterative clustering (SLIC) [1] generates superpixels relatively faster than other methods.

SLIC speed performance depends on a number of superpixels and the size of an image. Considering the size of

image constant, the number of superpixels plays as the key parameter. Having N superpixels divides the image to N initial squares and associate the center of each square as the cluster center. This center should not be on an edge of an object; therefore, the center is transferred to the lowest gradient position in a 3×3 neighborhood. Based on color information of each pixel with its nearest cluster centers, the pixel would be associated with a cluster center. It means that two coordinate components (x and y) depict the location of the segment and three components (for example in the RGB color space, R , G , and B) are derived from color channels. SLIC calculates a distance (an Euclidean norm on 5D spaces) function, which is defined as follow, and try to match the pixels based on this function.

$$D_c = \sqrt{(R_j - R_i)^2 + (G_j - G_i)^2 + (B_j - B_i)^2}, \quad (1)$$

$$D_p = \sqrt{(x_j - x_i)^2 + (y_j - y_i)^2}, \quad (2)$$

$$D = \sqrt{\left(\frac{D_c}{N_c}\right)^2 + \left(\frac{D_p}{N_p}\right)^2}. \quad (3)$$

where N_c and N_p are respectively maximum distances within a cluster used to normalized the color and spatial proximity. SLIC calculates this function for the cluster centers located in twice width of the initial square to minimize the calculation process.

The results of superpixel segmentation with four different SLIC superpixel numbers on a sample frame captured from a rat by five markers supposed to be drawn on the body is illustrated in Figure 1. Although, six markers were drawn because of a human error in the drawing. This frame was intentionally selected to show that a high number of superpixels can help us to segment the small markers and fix the human error for drawing the markers. The human error like this would not affect the segmentation and tracking; however, it can affect the tracking if they, the mistake and real marker, would be too close to each other (less than 10 pixels) which makes it impossible to differentiate them in some cases. Fortunately, a mistake like this is rare.

2.3. Direct Linear Transform

Direct linear transform (DLT) has been proposed to calibrate cameras for generating 3D reconstruction from the captured frames [14, 34]. It has been used to create a 3D model of objects in different applications, especially in biology and biomechanics worlds [3, 15, 16, 40, 38].

Figure 2 shows how an object can be projected to the camera image plane. O with $[x, y, z]$ is the an object in 3D space. $N1$ with $[x_1, y_1, z_1]$ and $N2$ with $[x_2, y_2, z_2]$ are the camera projection point which they project the object to $I1$ with $[U1, V1]$ coordinate in the image plane of camera 1 (the $U1V1$ space) and $I2$ with $[U2, V2]$ coordinate in the

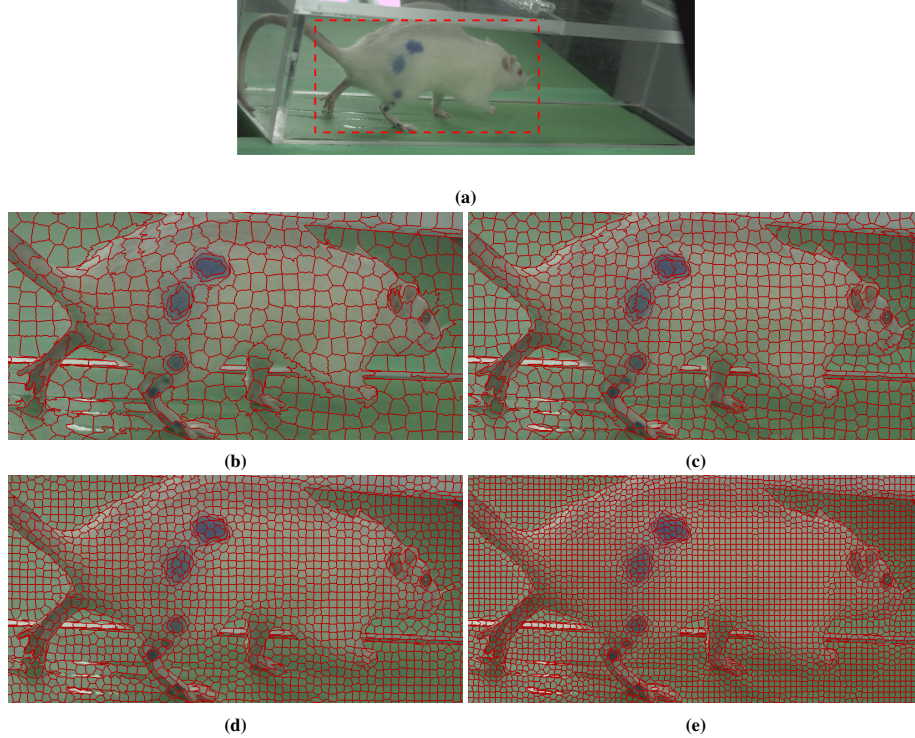


Figure 1. A sample video frame of rat locomotion with five markers drawn on the right side of an animal. A shows the original frame with the drawn red rectangle showing a region of a frame which is zoomed in for a better visualization. B, c, d, and e illustrate the zoomed in area from image (a) with 1250, 2500, 5000, and 10000 superpixels.

image plane of camera 2 (the $U2V2$ space). DLT gives the following relation between the object coordinate and projected object on the image plane from camera 1:

$$U1 = \frac{L1X + L2Y + L3Z + L4}{L9X + L10Y + L11Z + 1} \quad (4)$$

$$U2 = \frac{L5X + L6Y + L7Z + L8}{L9X + L10Y + L11Z + 1} \quad (5)$$

To find $L1$ to $L11$, it is needed to calibrate the cameras. Camera calibration should be done using a calibration object having some specific markers with known coordinates. We used a custom-made Lego with attached balls on top. This Lego can be seen in Figure 3.

2.4. 3D Kalman Filter

Kalman filter for motion analysis uses some observed measurements over time and estimates variables related to the motion. Kalman filter have been used frequently to predict the position of objects in different fields, human tracking [21], mice tracking [39], or cardiovascular disease detection [2]. The Kalman filter model assumes that the state of a system for a frame n evolved from the prior state at frame $n-1$ as follow [18]:

$$xn = Anxn_{-1} + Bnx_{n-1} + CnEn + Dn \quad (6)$$

where x , E , and t are the position of object, external force causing changes in position, and frame number. A , B , C , and D are four coefficients for each frame. We considered that there is no external and acceleration causing changes in our system to simplify the system. Considering having three dimensions, we got the following equations:

$$\begin{aligned} Xn &= B1_n X_{n-1} + D1_n \\ Yn &= B2_n Y_{n-1} + D2_n \\ Zn &= B3_n Z_{n-1} + D3_n \end{aligned} \quad (7)$$

where X , Y , Z are the coordinates in the object space seen in Figure 2. Therefore, our system had three states and three measurements to update the coefficients.

2.5. Features

Seven features were extracted from each superpixel to find an object having the best match with the previous detected landmarks. These seven features can be formalized

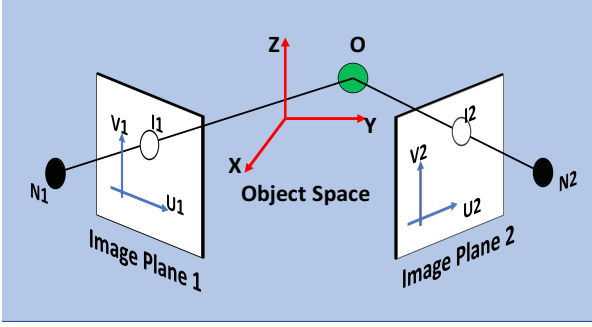


Figure 2. This figure shows how two camera can be used to extract the DLT coefficients from those two cameras image plane. O is the object located in a 3D object space with X , Y , and Z coordinate system. $N1$ and $N2$ are the projection point in camera 1 and 2, respectively. $I1$ and $I2$ are the projected points of object in image plane 1 and 2, respectively.

as follow:

$$\begin{aligned}
 F_{1[i,m,n]} &= Mean(SSP_{[i,n]}) - Mean(SD_{[m,n-1]}) \\
 F_{2[i,m,n]} &= Mean(SSP_{[i,n]}) - Mean(SD_{[m,0]}) \\
 F_{3[i,m,n]} &= Mean(HSP_{[i,n]}) - Mean(HD_{[m,n-1]}) \\
 F_{4[i,m,n]} &= Mean(HSP_{[i,n]}) - Mean(HD_{[m,0]}) \\
 F_{5[i,m,n]} &= Mean(GSP_{[i,n]}) - Mean(GD_{[m,n-1]}) \\
 F_{6[i,m,n]} &= Mean(GSP_{[i,n]}) - Mean(GD_{[m,0]}) \\
 F_{7[i,m,n]} &= sqrt([Mean(USP_{[i,n]}) - Mean(UP_{[m,n]})]^2 + \\
 &\quad [Mean(VSP_{[i,n]}) - Mean(VP_{[m,n]})]^2) \quad (8)
 \end{aligned}$$

where i , m , and n are the superpixel number (for all superpixels in a sub-image), the marker number (five markers), and the frame number (1000 frames in our studies for each trial). $SP_{[i,n]}$, $D_{[m,n]}$, and $P_{[m,n]}$ are the superpixel number i for the frame n , the detected landmark number m for frame number n , and the predicted position of landmark number m for frame number n . $F_{1[i,m,n]}$ to $F_{7[i,m,n]}$ are the seven features corresponding to $SP_{[i,n]}$. In addition, S , H , G , U , and V are saturation channel from the HSV color space [12], hue channel from the HSV color space [23], gray scale intensity, horizontal coordinate in the image plane (Figure 2), and vertical coordinate in the image plane (Figure 2), respectively.

2.6. Initial Tracker

The initial tracker was a simple step but necessary to initialize the marker position for two consecutive frames. Two frames from each camera were needed to update the Kalman filter coefficients as speed was needed to be calculated. The frames captured from every two Cameras located on the same side were processed at the same time to have a DLT based 3D reconstruction model.

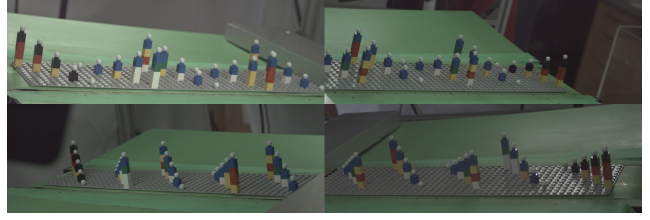


Figure 3. The calibration objects used for extracting the DLT coefficients. The calibration object had 25 balls located at different heights and locations with known coordinates relative to one of the balls, the one located on a corner with the lowest height.

The Initial tracker generated superpixels, by an initial value for the number of superpixels, asking a user to zoom in for a better resolution and click on the five landmarks for the first frame from each camera. Then, the maximum and minimum of all five landmarks coordinates on an image plane were calculated. This maximum and minimum numbers in each direction (U and V) were added by 100 to make sure that not missing the marker for the next frame. A smaller sub-image was extracted to reduce the required time for performing SLIC superpixels method. The features described in section 2.5 would be extracted and created the initial values needed in equation 8. Finally, the user was asked to click the markers for the second time. The rest of frames were processed using the method described in section 2.7.

2.7. General Tracker

We subsequently focused on a 100×100 pixel region of interest (ROI) given by the 2D projection of the 3D coordinate predicted using 3D Kalman filter described in section 2.4. This point has 2D coordinates of $[UP_{[m,n]}, VP_{[m,n]}]$ in the image plane for the marker number m and frame number n which it was used in equation 8 for calculation of $F_{7[i,m,n]}$. This zoomed in the region is referred as sub-image. The size of the image was selected based on the maximum displacement of the center of the body in rats (50 pixels); the same number can be applied to mice too.

By applying the SLIC method on each of these sub-images, the features described in section 2.5 were extracted for each of superpixels. One of the options for having these features was using a classifier like support vector or neural network as we presented a method for mice paw tracking using thresholding segmentation and both classifiers [11]. However, it should be reminded that the markers might have different intensities and even colors which makes the usage of a classifier limited as a tracker.

Therefore, we developed a probabilistic function, inspired by the one we presented in [11], to help us for tracking. First, to normalize the features and have the probabilistic function, we subtracted the $min(F_{k[Vi,m,n]})$ from the data and divided the data by the range ($max(F_{k[Vi,m,n]})$)

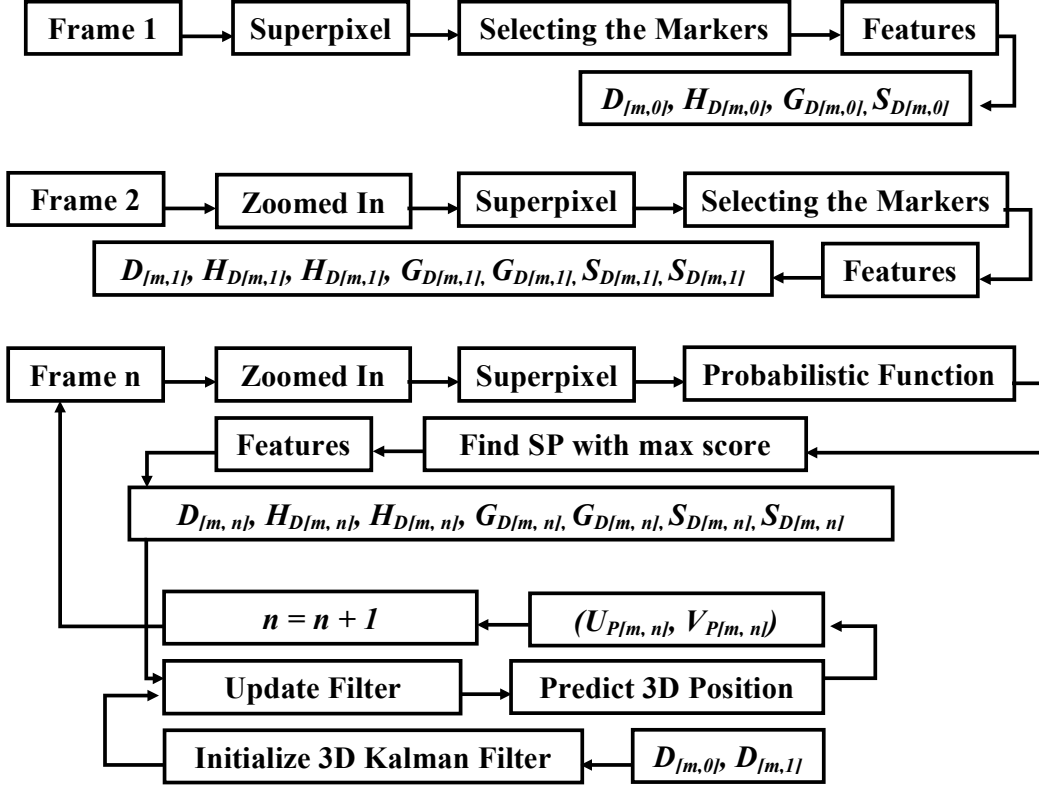


Figure 4. The calibration objects used for extracting the DLT coefficients. The calibration object had 25 balls located at different heights and locations with known coordinates relative to one of the balls, the one located on a corner with the lowest height.

- $\min(F_{k[\forall i,m,n]})$) where k, max, min are the feature number, maximum function, and minimum function, respectively. Therefore, the normalized feature (N) can be written as follow:

$$N_{k[i,m,n]} = \frac{F_{k[i,m,n]} - \min(F_{k[\forall i,m,n]})}{\max(F_{k[\forall i,m,n]}) - \min(F_{k[\forall i,m,n]})} \quad (9)$$

The normalized features are weighted based on the importance of features using the following array:

$$W = [3, 1, 3, 2, 2, 1, 3] \quad (10)$$

Then, each of $F_{k[\forall i,m,n]}$ should be multiplied by the corresponding $W[k]$ for $\forall k$. then the sum of this product would be calculated and the supersixel having the maximum number would be considered as the marker for the that frame. This can be formalized as follow:

$$S_{[i,m,n]} = \sum_{\forall k} (N_{k[i,m,n]} \times W[k]) \quad (11)$$

$$D_{[m,n]} = S_{[Ind(max(S_{[i,m,n]})),m,n]} \quad (12)$$

where $S_{[i,m,n]}$ is the sum of weighted features of the marker m calculated for the frame n . $Ind()$ finds the index of $S_{[i,m,n]}$ which is equal by $\max(S_{[i,m,n]})$. The process for tracking is illustrated in Figure 4.

3. Results

The method was examined using Python 2.7.12 platform with installed OpenCV 3.1.0-dev on a MacBook pro 2.7 GHz Intel Core i5 with 8 GB 1867 MHz DDR3.

Applying SLIC supersixel method on the frame or the generated sub-images, to reduce the required time for the supersixel process [1, 26], was the segmentation process as illustrated in Figure 4. As shown in Figure 1, the number of supersixels plays an important role in how the SLIC method would be performed. We had a comprehensive discussion on how we can select the correct supersixel number based on the size of markers [26]. If the size of marker would be a known parameter, then, the following equation can find the best supersixel number (NSLIC):

$$NSLIC = \frac{2048 \times 700}{NP} \times \frac{1}{100 \times 100 \times 2} \quad (13)$$

where NP is the number of pixels for that marker. 2048, 700, and 100 are the image width, height, and sub-image window size, respectively. Equation 13 can provide an ideal number of supersixels for SLIC; however, we needed an estimation of the size as the SLIC can segment the objects with half up to twice of initial size. Therefore, we considered 10,000, 10,000, 7,000, 3,000, and 3,000 as a number of

Table 1. Tracking results. The "SLIC + 3D Tracking" is the method presented here which is compared with three methods; "SLIC + 2D Tracking" [26], "Thre + 2D Tracking" [26], and "Manual Tracking". "SLIC" and "Thre" are superpixel method presented in [1] and the thresholding on the hue channel. There are eight small tables showing different conditions for evaluation of the method. From top to bottom the small tables show: the number of frame and markers for the whole database used here; average time was required for each method to process one trial (1000 frames); the results for tracking of the markers drawn bad or unclear, the tracking results when the markers were unclear or hidden from the beginning; the tracking results while a marker was partially occluded; the results when the markers were completely occluded; the results when a perfect consequence of frames are next to each other; the comprehensive results considering all mistakes and conditions excluding the "Missing Start".

Method	Manual Tracking	Thre + 2D Tracking	SLIC + 2D Tracking	SLIC + 3D Tracking
Database Frames	1,000	4,000	4,000	24,000
Database Markers	5,000	20,000	20,000	120,000
Average Time per Trial	8,700 ± 2300	108 ± 12	118 ± 14	149 ± 18
Bad Marker Frames	-	800	800	13,500
Total Bad Markers	-	800	800	13,500
Correct Tracked	-	23	127	11,582
Percentage	100	2.88	15.87	85.79
Missing Start	100	400	400	2,200
Total Markers	500	2,000	2,000	11,000
Correct Tracked	500	35	59	1319
Percentage	100	1.75	2.95	11.99
Partitially Occluded	30	250	250	4,500
Total Markers	150	1,250	1,250	22,500
Correct Tracked	150	10	217	21,212
Percentage	100	0.8	17.36	94.28
Occluded	50	300	300	5,100
Total Markers	250	1,500	1,500	25,500
Correct Tracked	250	10	217	22,788
Percentage	100	0.67	14.47	89.36
Perfect Consecutive	450	1,300	1,300	8,100
Total Markers	2,250	6,500	6,500	40,500
Correct Tracked	2,250	6,377	6,494	40,496
Percentage	100	98.11	99.90	99.99
Total Frames	900	3,600	3,600	21,800
Total Markers	4,500	18,000	18,000	109,000
Correct Tracked	4,500	10,891	14,237	103,562
Percentage	100	60.50	79.09	95.01

superpixels of a frame, *NSLIC*, for toe, ankle, knee, hip, and anterior superior iliac spine markers, respectively.

The segmentation process using the SLIC superpixel method was examined in [26].

As discussed in the introduction, manual tracking can be considered as the common method to track the markers for many applications in biomechanics. To compare how the proposed method can be helpful for biomechanics/neuroscience applications; we compare this method with manual tracking, thresholding for segmentation and 2D tracking, SLIC method for segmentation and 2D tracking [26], SLIC method for segmentation and 3D tracking.

The method was examined in six Sprague-Dawley rats. Each rat had five markers showing: toe, ankle, knee, hip, and anterior superior iliac spine. We randomly selected two trails from each rat and each trial contained 1,000 frames. It created 12,000 from each of the two cameras capturing the right side of the animal, the five markers were drawn on the right side. Therefore, total 24,000 frames producing 120,000 markers consist of this study database.

We evaluated the method for different conditions: bad marker frames, the marker was painted poorly causing difficulties in finding them; missing start, a trial starts with a set of markers barely being visualized but still user initialized

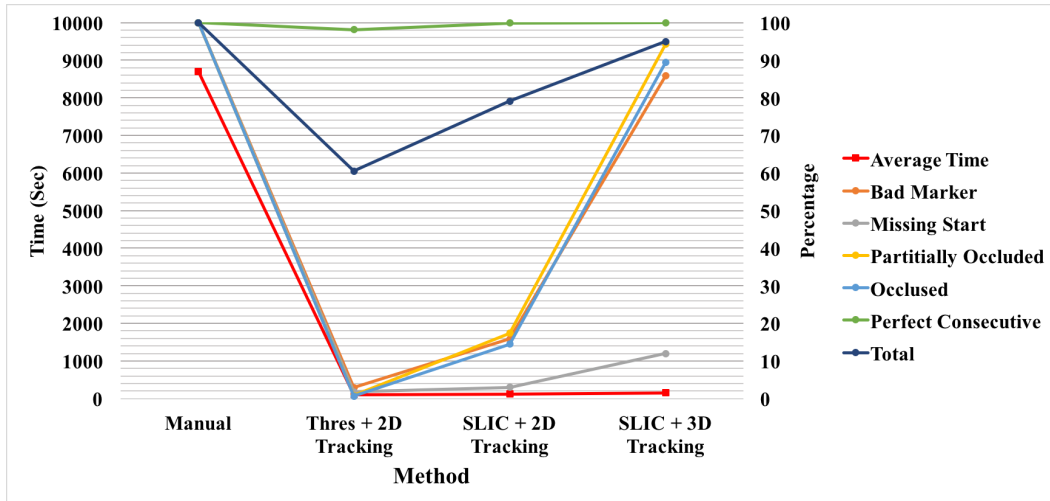


Figure 5. A comparison between the methods. Manual tracking, thresholding following by 2D tracking, SLIC following by 2D tracking, and the method presented here are compared with each other. The Average time to process a trial, 1,000 frames, is graphed in red. The average time is on the left axis and the rest of plots are on the right axis.

the marker location by guessing the position; partially occluded, the markers were partially occluded by body or dirt on the plexy glass; occluded, the markers were completely occluded; perfect consecutive, a consequence of frames that the markers were clear for whole time; total frames, the total results were reported.

The results for all these conditions are separately illustrated in Table 1 and Figure 5. In addition, Figure 6 shows a 3D reconstructed video from a rat while running on the treadmill.

It should be noted that we did not add the required time for finding the DLT coefficients in the results presented here.

4. Conclusion

We presented a method to segment the drawn markers on the body of rats using SLIC superpixel method following by a 3D Kalman based tracker to predict the position of markers in a 3D domain and projecting them to the 2D image plane. Having the coordinates on the 2D image plane and assigning a score to each of the superpixels based on the predicted coordinate, color, and texture information of marker in the previous frame provided us the ability to use a probabilistic function 4.

The method was evaluated 24 trails and 5 markers drawn on the body of an animal. We compared the method with available methods [26] utilizing simple thresholding or superpixel method followed by 2D tracker based.

The results showed that the best method, as expected, was using manual tracking; however, it takes so much time to process one trail. It shows the importance of using an accurate method for marker tracking. In addition, the manual

tracking involves intraobserver and interobserver tracking error which was not studied here.

The 3D tracking showed its superiority compared with 2D tracking methods in all conditions. However, the results show that if there would be a perfect consequence of frames, the superpixel method using 2D tracking can work the same as 3D based tracking method while it is slightly faster than 3D based tracking method. It should be reminded that the required time to calculate the DLT coefficients was not involved in the time plot in Table 1. However, it is hard to find perfect consequence of frames when capturing from the animal.

Our future study would be developing 3D based tracker for a markerless animal to avoid handling and painting of markers on the body of the animal. The painting a marker needs long anesthesia for mice following by bleaching and drawing markers. In addition, we will try to use a 3D model of markers to reduce the miss-tracking. Having a 3D model can provide a good setup to track the markers based on the other markers. It means that we can find the markers missing or wrongly labeled using the other markers.

References

- [1] R. Achanta, A. Shaji, K. Smith, A. Lucchi, P. Fua, and S. Süsstrunk. Slic superpixels compared to state-of-the-art superpixel methods. *IEEE transactions on pattern analysis and machine intelligence*, 34(11):2274–2282, 2012.
- [2] J. Bersvendsen, F. Orderud, R. J. Massey, K. Fosså, O. Gerard, S. Urheim, and E. Samset. Automated segmentation of the right ventricle in 3d echocardiography: a kalman filter state estimation approach. *IEEE transactions on medical imaging*, 35(1):42–51, 2016.

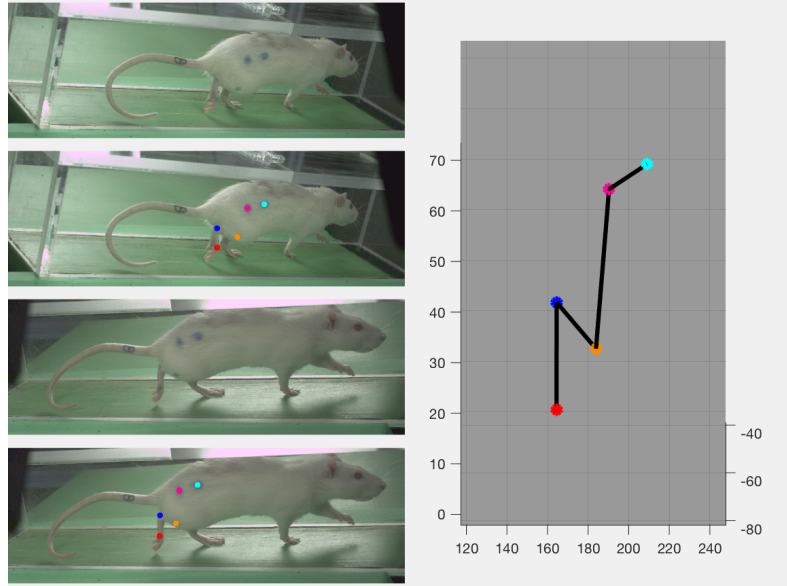


Figure 6. A video of tracked markers for 1,000 consecutive frames using the presented method here. (MP4 14.6MB). Left frames from top to bottom show a captured frame from camera 3, tracked markers for the corresponding frame from camera 3, a captured frame from camera 4, and tracked markers for the corresponding frame from camera 4. The right image shows the 3D reconstruction of markers using the DLT coefficients.

- [3] A. M. Choo and T. R. Oxland. Improved rsa accuracy with dlt and balanced calibration marker distributions with an assessment of initial-calibration. *Journal of biomechanics*, 36(2):259–264, 2003.
- [4] D. Comaniciu and P. Meer. Mean shift: A robust approach toward feature space analysis. *IEEE Transactions on pattern analysis and machine intelligence*, 24(5):603–619, 2002.
- [5] K. Deisseroth. Optogenetics. *Nature methods*, 8(1):26–29, 2011.
- [6] R. Deumens, R. J. Jaken, M. A. Marcus, and E. A. Joosten. The catwalk gait analysis in assessment of both dynamic and static gait changes after adult rat sciatic nerve resection. *Journal of neuroscience methods*, 164(1):120–130, 2007.
- [7] C. W. Dorman, H. E. Krug, S. P. Frizelle, S. Funkenbusch, and M. L. Mahowald. A comparison of digigait and treadscan imaging systems: assessment of pain using gait analysis in murine monoarthritis. *Journal of pain research*, 7:25, 2014.
- [8] P. F. Felzenszwalb and D. P. Huttenlocher. Efficient graph-based image segmentation. *International journal of computer vision*, 59(2):167–181, 2004.
- [9] K. K. Gadalla, P. D. Ross, J. S. Riddell, M. E. Bailey, and S. R. Cobb. Gait analysis in a mecp2 knockout mouse model of rett syndrome reveals early-onset and progressive motor deficits. *PloS one*, 9(11):e112889, 2014.
- [10] O. Haji-Maghsoudi, A. Talebpour, H. Soltanian-Zadeh, and N. Haji-maghsoudi. Automatic organs’ detection in wce. In *Artificial Intelligence and Signal Processing (AISP), 2012 16th CSI International Symposium on*, pages 116–121. IEEE, 2012.
- [11] O. HajiMaghsoudi, A. V. Tabrizi, B. Robertson, P. Shamble, and A. Spence. Support vector machine and neural network based trackers for rodent locomotion. *IET Image Processing*.
- [12] O. HajiMaghsoudi, A. Talebpour, H. Soltanian-zadeh, and H. A. Soleimani. Automatic informative tissue’s discriminators in wce. In *Imaging Systems and Techniques (IST), 2012 IEEE International Conference on*, pages 18–23. IEEE, 2012.
- [13] F. P. Hamers, A. J. Lankhorst, T. J. van Laar, W. B. Veldhuis, and W. H. Gispen. Automated quantitative gait analysis during overground locomotion in the rat: its application to spinal cord contusion and transection injuries. *Journal of neurotrauma*, 18(2):187–201, 2001.
- [14] H. Hatze. High-precision three-dimensional photogrammetric calibration and object space reconstruction using a modified dlt-approach. *Journal of biomechanics*, 21(7):533–538, 1988.
- [15] T. L. Hedrick. Software techniques for two-and three-dimensional kinematic measurements of biological and biomimetic systems. *Bioinspiration & biomimetics*, 3(3):034001, 2008.
- [16] T. L. Hedrick, B. W. Tobalske, I. G. Ros, D. R. Warrick, and A. A. Biewener. Morphological and kinematic basis of the hummingbird flight stroke: scaling of flight muscle transmission ratio. In *Proc. R. Soc. B*, volume 279, pages 1986–1992. The Royal Society, 2012.
- [17] P. Huehnen, W. Boehmerle, and M. Endres. Assessment of paclitaxel induced sensory polyneuropathy with catwalk automated gait analysis in mice. *PloS one*, 8(10):e76772, 2013.

- [18] R. E. Kalman et al. A new approach to linear filtering and prediction problems. *Journal of basic Engineering*, 82(1):35–45, 1960.
- [19] A. Levinshstein, A. Stere, K. N. Kutulakos, D. J. Fleet, S. J. Dickinson, and K. Siddiqi. Turbopixels: Fast superpixels using geometric flows. *IEEE transactions on pattern analysis and machine intelligence*, 31(12):2290–2297, 2009.
- [20] Z. Li, X.-M. Wu, and S.-F. Chang. Segmentation using superpixels: A bipartite graph partitioning approach. In *Computer Vision and Pattern Recognition (CVPR), 2012 IEEE Conference on*, pages 789–796. IEEE, 2012.
- [21] G. Ligorio and A. M. Sabatini. A novel kalman filter for human motion tracking with an inertial-based dynamic inclinometer. *IEEE Transactions on Biomedical Engineering*, 62(8):2033–2043, 2015.
- [22] Z. Ma and A. B. Chan. Counting people crossing a line using integer programming and local features. *IEEE Transactions on Circuits and Systems for Video Technology*, 26(10):1955–1969, 2016.
- [23] O. H. Maghsoudi, M. Alizadeh, and M. Mirmomen. A computer aided method to detect bleeding, tumor, and disease regions in wireless capsule endoscopy. In *Signal Processing in Medicine and Biology Symposium (SPMB), 2016 IEEE*, pages 1–6. IEEE, 2016.
- [24] O. H. Maghsoudi, A. V. Tabrizi, B. Robertson, P. Shamble, and A. Spence. A novel automatic method to track the body and paws of running mice in high speed video. In *Signal Processing in Medicine and Biology Symposium (SPMB), 2015 IEEE*, pages 1–2. IEEE, 2015.
- [25] O. H. Maghsoudi, A. V. Tabrizi, B. Robertson, P. Shamble, and A. Spence. A rodent paw tracker using support vector machine. In *Signal Processing in Medicine and Biology Symposium (SPMB), 2016 IEEE*, pages 1–3. IEEE, 2016.
- [26] O. H. Maghsoudi, A. V. Tabrizi, B. Robertson, and A. Spence. Superpixels based marker tracking vs. hue thresholding in rodent biomechanics application. *arXiv preprint arXiv:1710.06473*, 2017.
- [27] A. Mahdi, H. Omid, S. Kaveh, R. Hamid, K. Alireza, and T. Alireza. Detection of small bowel tumor in wireless capsule endoscopy images using an adaptive neuro-fuzzy inference system. *Journal of biomedical research*, 2017.
- [28] A. A. Migliaccio, R. Meierhofer, and C. C. Della Santina. Characterization of the 3d angular vestibulo-ocular reflex in c57bl6 mice. *Experimental brain research*, 210(3-4):489–501, 2011.
- [29] G. Mori, X. Ren, A. A. Efros, and J. Malik. Recovering human body configurations: Combining segmentation and recognition. In *Computer Vision and Pattern Recognition, 2004. CVPR 2004. Proceedings of the 2004 IEEE Computer Society Conference on*, volume 2, pages II–II. IEEE, 2004.
- [30] S. Nori, Y. Okada, S. Nishimura, T. Sasaki, G. Itakura, Y. Kobayashi, F. Renault-Mihara, A. Shimizu, I. Koya, R. Yoshida, et al. Long-term safety issues of ipsc-based cell therapy in a spinal cord injury model: oncogenic transformation with epithelial-mesenchymal transition. *Stem Cell Reports*, 4(3):360–373, 2015.
- [31] S. S. Parvathy and W. Masocha. Gait analysis of c57bl/6 mice with complete freund’s adjuvant-induced arthritis using the catwalk system. *BMC musculoskeletal disorders*, 14(1):14, 2013.
- [32] R. Penjweini, S. Deville, O. Haji Maghsoudi, K. Notelaers, A. Ethirajan, and M. Ameloot. Investigating the effect of poly-l-lactic acid nanoparticles carrying hypericin on the flow-biased diffusive motion of hela cell organelles. *Journal of Pharmacy and Pharmacology*, 2017.
- [33] D. F. Preisig, L. Kulic, M. Krüger, F. Wirth, J. McAfoose, C. Späni, P. Gantenbein, R. Derungs, R. M. Nitsch, and T. Welt. High-speed video gait analysis reveals early and characteristic locomotor phenotypes in mouse models of neurodegenerative movement disorders. *Behavioural brain research*, 311:340–353, 2016.
- [34] B. Přibyl, P. Zemčík, and M. Čadík. Absolute pose estimation from line correspondences using direct linear transformation. *Computer Vision and Image Understanding*, 2017.
- [35] X. Ren and J. Malik. Learning a classification model for segmentation. In *ICCV*, volume 1, pages 10–17, 2003.
- [36] B. L. Roth. Dreads for neuroscientists. *Neuron*, 89(4):683–694, 2016.
- [37] T. Schubert, A. Gkogkidis, T. Ball, and W. Burgard. Automatic initialization for skeleton tracking in optical motion capture. In *Robotics and Automation (ICRA), 2015 IEEE International Conference on*, pages 734–739. IEEE, 2015.
- [38] J. Song, H. Luo, and T. L. Hedrick. Three-dimensional flow and lift characteristics of a hovering ruby-throated hummingbird. *Journal of The Royal Society Interface*, 11(98):20140541, 2014.
- [39] A. J. Spence, G. Nicholson-Thomas, and R. Lampe. Closing the loop in legged neuromechanics: an open-source computer vision controlled treadmill. *Journal of neuroscience methods*, 215(2):164–169, 2013.
- [40] D. H. Theriault, N. W. Fuller, B. E. Jackson, E. Bluhm, D. Evangelista, Z. Wu, M. Betke, and T. L. Hedrick. A protocol and calibration method for accurate multi-camera field videography. *Journal of Experimental Biology*, pages jeb-100529, 2014.
- [41] O. Veksler, Y. Boykov, and P. Mehrani. Superpixels and supervoxels in an energy optimization framework. In *European conference on Computer vision*, pages 211–224. Springer, 2010.
- [42] Z. Wu, N. I. Hristov, T. L. Hedrick, T. H. Kunz, and M. Betke. Tracking a large number of objects from multiple views. In *Computer Vision, 2009 IEEE 12th International Conference on*, pages 1546–1553. IEEE, 2009.